



## Selective catalytic reaction of $\text{NO}_x$ with $\text{NH}_3$ over Ce–Fe/TiO<sub>2</sub>-loaded wire-mesh honeycomb: Resistance to SO<sub>2</sub> poisoning



Yun Shu, Tanana Aikebaier, Xie Quan\*, Shuo Chen, Hongtao Yu

*Key Laboratory of Industrial Ecology and Environmental Engineering, Ministry of Education, China, School of Environmental Science and Technology, Dalian University of Technology, Dalian 116024, China*

### ARTICLE INFO

#### Article history:

Received 8 November 2013

Received in revised form

24 December 2013

Accepted 4 January 2014

Available online 10 January 2014

#### Keywords:

SCR

Wire-mesh honeycomb catalyst

Surface sulfation

Resistance to SO<sub>2</sub>

### ABSTRACT

Ce–Fe/TiO<sub>2</sub>/Al<sub>2</sub>O<sub>3</sub>/wire-mesh honeycomb catalyst (Ce–Fe/WMH) exhibited a high activity for the selective catalytic reduction (SCR) of  $\text{NO}_x$  in SO<sub>2</sub>-containing gases. Analysis of fresh and spent catalysts by XRD, BET, XPS, TG and FTIR indicated that Ce sites were sulfated preferentially over Ce–Fe/WMH during the SCR reaction in the presence of SO<sub>2</sub>, which could increase the amount of surface active oxygen species. On the other hand, the formation of surface hydroxyls due to the hydration of SO<sub>4</sub><sup>2-</sup> could supply more Brønsted acid sites to adsorb NH<sub>3</sub> in the form of NH<sub>4</sub><sup>+</sup>. These two factors played significant roles in the good SO<sub>2</sub> durability of Ce–Fe/WMH. In addition, the sulfation of CeO<sub>2</sub> on catalyst surface might approach a stable state upon certain amount of SO<sub>2</sub> in reactant gas. The reaction mechanism study showed that only Eley–Rideal reaction pathway between ionic NH<sub>4</sub><sup>+</sup>, coordinated NH<sub>3</sub> and gaseous NO dominated in the reaction; the Langmuir–Hinshelwood reaction pathway was cut off by the sulfation, resulting in the rapid decrease of  $\text{NO}_x$  conversion in the early period of SCR reaction in the presence of SO<sub>2</sub>.

© 2014 Elsevier B.V. All rights reserved.

### 1. Introduction

Selective catalytic reduction (SCR) with ammonia is considered to be the most efficient and widely used technology for reducing  $\text{NO}_x$  emissions from stationary sources, such as power boilers and combustion furnaces. The commercial catalysts for this process are V<sub>2</sub>O<sub>5</sub>/TiO<sub>2</sub> (anatase) promoted by WO<sub>3</sub> or MoO<sub>3</sub>, and they are preferentially applied in form of monolithic honeycombs due to their low pressure drop [1–3]. However, these vanadium-based catalysts are not environmental friendly as the vanadium is harmful to ecological environment. Therefore, an urgent demand for developing environmentally-benign deNO<sub>x</sub> catalysts is put forward, and a lot of works have been performed to find new SCR catalyst systems, including zeolite [4,5] and transition metal oxides [6–8]. Recently, we also reported a Ce–Fe/TiO<sub>2</sub> catalyst [9], which was highly active in the SCR reaction within the temperature range of 160–350 °C.

Since typical coal fired exhaust contains variable amounts of SO<sub>2</sub> which can deactivate the SCR catalysts due to the formation of metal sulfate species [10] or the blockage of catalyst pore channels [11,12], understanding the effects of SO<sub>2</sub> on SCR activity is important for the development and application of appropriate catalysts.

Recently, some researchers reported that the catalysts would not be poisoned but significantly promoted by SO<sub>2</sub> [13–16]. All of these researchers agreed that the promoting role of SO<sub>2</sub> was resulted from the enhancement of NH<sub>3</sub> adsorption by the increase in surface acidity after sulfation. Upon sulfation of the catalyst, the acid sites increased in both number and strength. The latter was ascribed to the inductive effect of the S=O bond [17,18]. García-Bordejé et al. [19] also found that the sulfates formed could account for the improvement of the redox properties in the sulfated catalyst, which was beneficial for the reduction of NO with NH<sub>3</sub>. However, most of researchers tested the SCR activity in SO<sub>2</sub>-containing gases by changing the reaction temperature, which could not meet the demand of the practical application. The deactivation effect of SO<sub>2</sub> on SCR catalyst needs a long time to achieve steady state. It is thus necessary to investigate the influence of SO<sub>2</sub> on SCR activity in relatively long reaction time.

It is well known that the monolith catalyst is more representative in industrial application of NO reduction. Wire-mesh honeycomb is a new structured catalytic reactor, which combines the characteristics of wire mesh and monolith catalyst. In this work, a novel wire-mesh honeycomb-supported Ce–Fe/TiO<sub>2</sub> catalyst (Ce–Fe/WMH) was developed as a NH<sub>3</sub>-SCR catalyst. The SO<sub>2</sub> durability (100 h) of the Ce–Fe/WMH at 250 °C was investigated, and then the nature of sulfated species and the mechanism of reaction were studied over the sulfated catalyst.

\* Corresponding author. Tel.: +86 411 84706140; fax: +86 411 84706263.

E-mail address: [quanie@dlut.edu.cn](mailto:quanie@dlut.edu.cn) (X. Quan).

## 2. Experimental

### 2.1. Catalyst preparation

Wire-mesh honeycomb ( $35\text{ mm} \times 35\text{ mm} \times 10\text{ mm}$ ) was manufactured by stacking alternatively corrugated and plain wire mesh sheets, which contained 100 cells per square inch. As the bare surface of metal wire can hardly attach catalyst, the wire-mesh honeycomb substrate was coated with  $\text{Al}_2\text{O}_3$  powder by an electrophoretic deposition (EPD) method as described elsewhere [20,21]. The alumina suspension was prepared with  $\gamma$ -alumina powders gritted from  $\gamma$ -alumina pellets. Polycyclic acid and aluminum isopropoxide were used as additives. The resulting  $\text{Al}_2\text{O}_3$ /wire-mesh honeycomb has a BET surface area of  $87.5\text{ m}^2/\text{g}$  measured by  $\text{N}_2$  adsorption at  $77\text{ K}$ .

$\text{Ce}-\text{Fe}/\text{TiO}_2$  was supported on the  $\text{Al}_2\text{O}_3$ /wire-mesh honeycomb by a two-step impregnation method. The detailed preparation procedure was described in our previous work [21]. This includes four steps: (i) impregnating the  $\text{Al}_2\text{O}_3$ /wire-mesh honeycomb in a  $\text{TiO}_2$  slurry; (ii) drying at  $100^\circ\text{C}$ ; (iii) impregnating the  $\text{TiO}_2/\text{Al}_2\text{O}_3$ /wire-mesh honeycomb in an aqueous solution of cerium nitrate and iron nitrate; and (iv) drying at  $100^\circ\text{C}$  and calcining at  $500^\circ\text{C}$ . The resulting  $\text{Ce}-\text{Fe}/\text{TiO}_2/\text{Al}_2\text{O}_3$ /wire-mesh honeycomb catalyst was denoted as Ce–Fe/WMH, in which the  $\text{Ce}-\text{Fe}/\text{TiO}_2$  loading of catalyst was about  $130\text{ g/l}$ . The compositions of the  $\text{Ce}-\text{Fe}/\text{TiO}_2$  as determined by atomic absorption spectrometer (AAS) with graphite furnace (AAnalyst 700, PerkinElmer) were about 1.4 wt% Fe, 24.1 wt% Ce and 74.5 wt%  $\text{TiO}_2$ , respectively, and the thickness of the  $\text{Ce}-\text{Fe}/\text{TiO}_2$  washcoat was  $30\text{ }\mu\text{m}$  (as shown in Fig. S1).

### 2.2. Activity measurements

The catalytic studies were carried out in a square-shaped reactor ( $4.0\text{ cm} \times 4.0\text{ cm}$  in width) made of stainless steel with a total bed length of  $100\text{ cm}$ . The catalysts were placed inside the reactor in the middle. Free space between the catalyst and the reactor wall was filled with inert material to prevent bypass. The typical composition of the reactant gas was:  $1000\text{ ppm NO}$ ,  $1000\text{ ppm NH}_3$ ,  $3\%$   $\text{O}_2$ ,  $100\text{--}1000\text{ ppm SO}_2$  (when needed), and  $\text{N}_2$  as the balance gas. The total flow rate was  $2000\text{ ml/min}$  (refers to  $1\text{ atm}$  and  $298\text{ K}$ ) which corresponded to gas hourly space velocity (GHSV) of  $10,000\text{ h}^{-1}$ . The  $\text{NO}$ ,  $\text{NO}_2$  and  $\text{O}_2$  concentrations were measured online by a flue gas analyzer (ecom-J2KN, rbr Messtechnik GmbH Inc.). The  $\text{N}_2\text{O}$  was analyzed by a gas chromatograph (Shimadzu GC–14 C) with a Porapak Q column. The activities were evaluated in terms of  $\text{NO}_x$  conversion determined according to the following equation:

$$\text{NO}_x \text{ conversion} = \left( 1 - \frac{[\text{NO}_x]_{\text{out}}}{[\text{NO}_x]_{\text{in}}} \right) \times 100\%$$

where  $[\text{NO}_x] = [\text{NO}] + [\text{NO}_2]$ , and  $[\text{NO}_x]_{\text{in}}$  and  $[\text{NO}_x]_{\text{out}}$  were the concentrations of  $\text{NO}_x$  at the inlet and outlet of the reactor, respectively. In order to confirm that the decrease of  $\text{NO}_x$  was not caused by the adsorption of  $\text{NO}_x$  in the catalysts, at the beginning of each experiment, the catalyst was purged with the reactant gas until there was no difference between the inlet and the outlet gas.

### 2.3. Catalyst characterization

Scanning electron microscopy (SEM) of the catalyst was measured on a HITACHI S-4800 operating at  $3.0\text{ kV}$ . The specific surface areas of the catalysts were measured by nitrogen adsorption using the Brunauer–Emmett–Teller (BET) method (Quadasorb SI). Powder X-ray diffraction (XRD) measurements were carried out on a Rigaku D/MAX-2400 X-ray diffractometer with  $\text{Cu K}\alpha$  radiation. X-ray photoelectron spectroscopy (XPS) was implemented on a surface analysis system (Thermal ESCALAB 250) using  $\text{Al K}\alpha$  radiation.

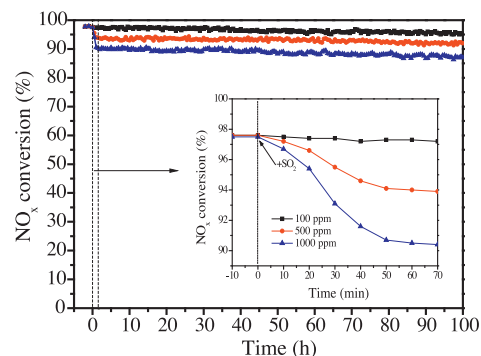


**Fig. 1.** Effect of  $\text{SO}_2$  on  $\text{NO}_x$  conversion of Ce–Fe/WMH catalyst. Reaction conditions:  $[\text{NO}] = [\text{NH}_3] = 1000\text{ ppm}$ ,  $[\text{O}_2] = 3\text{ vol\%}$ ,  $[\text{SO}_2] = 100, 500$  and  $1000\text{ ppm}$  (when used),  $\text{N}_2$  balance and GHSV =  $10,000\text{ h}^{-1}$ ,  $T = 250^\circ\text{C}$ .

The C 1s line at  $284.6\text{ eV}$  was considered as a reference for the binding energy calibration. Fourier transform infrared spectroscopy (FT-IR) was performed with Bruker Vector FTIR spectrometer used a DTGS detector. Before the analyses, about  $2\text{ mg}$  of the sample was ground, mixed, and palletized with pure KBr by a weight ratio of 1:100. Thermo gravimetric analysis (TGA) was carried out in a static  $\text{N}_2$  atmosphere, using a TG/DTA 6300 instrument. An amount of  $6\text{--}9\text{ mg}$  of each sample was analyzed between  $20$  and  $1000^\circ\text{C}$  at a rate of  $10^\circ\text{C}/\text{min}$ .

The in situ DRIFTS experiments were performed on a Bruker Vector FTIR spectrometer with in situ diffuse reflectance pool and high sensitivity MCT detector cooled by liquid  $\text{N}_2$ . An approximately  $12\text{ mg}$  sample was finely ground and pressed into a self-supported wafer. Mass flow controllers and a sample temperature controller were used to simulate the real reaction conditions. Prior to each experiment, the wafer was heated to  $350^\circ\text{C}$  in  $\text{N}_2$  (99.999%) for  $1\text{ h}$  and then cooled down to the desired reaction temperature. The background spectrum was collected in flowing  $\text{N}_2$  and automatically subtracted from the sample spectrum. The reaction conditions were controlled as follows:  $500\text{ ml/min}$  total flow rate,  $500\text{ ppm NO}$ ,  $500\text{ ppm NH}_3$ ,  $3\%$   $\text{O}_2$  and  $\text{N}_2$  balance. All spectra were recorded by accumulating 100 scans with a resolution of  $4\text{ cm}^{-1}$ .

## 3. Results and discussion

### 3.1. Effect of $\text{SO}_2$ on $\text{NO}_x$ conversion

Effects of  $\text{SO}_2$  (100–1000 ppm) on SCR activity of Ce–Fe/WMH at  $250^\circ\text{C}$  is illustrated in Fig. 1. Under the employed reaction condition without  $\text{SO}_2$ , a steady-state  $\text{NO}_x$  conversion of  $97.6\%$  was obtained. In the presence of  $100\text{ ppm SO}_2$ , there was almost no change of  $\text{NO}_x$  conversion over the catalyst in the tested  $100\text{ h}$ . However, when  $500\text{ ppm SO}_2$  was added to the feed,  $\text{NO}_x$  conversion decreased from  $97.6\%$  to  $93.9\%$  in the early  $50\text{ min}$  (inset of Fig. 1), and then it could maintained at about  $92\%$  for  $100\text{ h}$ . In the case of  $1000\text{ ppm SO}_2$ , an obvious decrease in  $\text{NO}_x$  conversion from  $97.6\%$  to  $90.3\%$  also occurred after  $50\text{ min}$  and then the conversion slightly decreased to  $88\%$  after  $100\text{ h}$ . These results demonstrated that the Ce–Fe/WMH exhibited good resistance to  $\text{SO}_2$  poisoning in the tested  $100\text{ h}$ . Interestingly, the  $\text{NO}_x$  conversion variation trends in the first  $50\text{ min}$  and following reaction time were different. It was inferred that the obvious decrease after the addition of  $\text{SO}_2$  (500,  $1000\text{ ppm}$ ) was ascribed to the competitive adsorption of  $\text{NO}$  and  $\text{SO}_2$ . Since  $\text{SO}_2$  and  $\text{H}_2\text{O}$  are present in the exhausts, the durability of  $\text{SO}_2$  and  $\text{H}_2\text{O}$  was also studied on Ce–Fe/WMH (as shown in Fig. S2). It could be seen that the  $\text{NO}_x$  conversion retained about  $70\%$  at least for  $100\text{ h}$  in the presence of  $1000\text{ ppm SO}_2$  and  $10\%\text{ H}_2\text{O}$  at

**Table 1**

Surface atomic concentrations and binding energies of fresh and spent Ce–Fe/WMH catalysts.

Catalyst	Surface atomic concentration (%)					Binding energy (eV)	
	Ce	Fe	Ti	O	S	Ce 3d <sub>5/2</sub> (v)	Ce 3d <sub>3/2</sub> (u)
Ce–Fe/WMH	3.53	2.55	24.76	69.16	—	883.1	904.9
Ce–Fe/WMH(100 ppm)	3.62	1.85	16.52	72.16	5.85	882.8	904.3
Ce–Fe/WMH(500 ppm)	3.37	1.77	16.06	71.09	7.71	882.5	904.5
Ce–Fe/WMH(1000 ppm)	3.19	1.70	15.64	71.83	7.64	882.7	904.6

250 °C. Therefore, the Ce–Fe/WMH showed promising resistance to water vapor and SO<sub>2</sub> poisoning.

### 3.2. Characterization of fresh and spent catalysts

The X-ray diffraction patterns of the fresh Ce–Fe/WMH, Ce–Fe/WMH (100 ppm), Ce–Fe/WMH (500 ppm) and Ce–Fe/WMH (1000 ppm) catalysts are shown in Fig. 2, here the Ce–Fe/WMH ( $x$  ppm) refers to a spent catalyst tested in a reactant gas containing  $x$  ppm SO<sub>2</sub>. Fresh Ce–Fe/WMH provided typical diffraction patterns for the cubic CeO<sub>2</sub> structure (PDF no. 34-0394), TiO<sub>2</sub> anatase phase (PDF no. 21-1272) and a little rutile phase (PDF no. 21-1276). For all the spent catalysts, no obvious change was observed in the lattice parameters of anatase and rutile, but the intensity of the diffraction peaks of cubic CeO<sub>2</sub> was slightly decreased, suggesting a loss of CeO<sub>2</sub> crystallinity after reactions in SO<sub>2</sub>-containing gases. Moreover, no extra peaks ascribed to sulfated phase were observed in the XRD patterns, which indicated that the sulfated species might exist as either surface sulfate or amorphous bulk sulfate.

In order to indentify the state of surface species after SCR reaction in the presence of SO<sub>2</sub>, the catalysts were examined by XPS spectroscopy. The surface atomic concentrations of Ce, Fe, Ti, O and S, together with the binding energies of Ce 3d<sub>5/2</sub> (v) and Ce 3d<sub>3/2</sub> (u), are summarized in Table 1. In comparison with the fresh Ce–Fe/WMH, the spent catalysts showed a decrease in the surface concentrations of Ce, Fe and Ti.

Fig. 3(A) reveals the S 2p spectra of fresh and spent Ce–Fe/WMH catalysts. On the fresh Ce–Fe/WMH, no obvious S 2p band was observed, while an evident band attributed to S 2p was observed on all the spent catalysts. The binding energy of this S 2p band was 169.2 eV, which was consistent with the S (VI) oxidation state and assigned to the inorganic sulfate with ionic S–O bands [22,23]. Furthermore, the sulfur contents for Ce–Fe/WMH (100 ppm), Ce–Fe/WMH (500 ppm) and Ce–Fe/WMH (1000 ppm) were 5.85%, 7.71% and 7.64%, respectively (as shown in Table 1), revealing that the relative amount of sulfate did not increase with the concentration of SO<sub>2</sub> in reactant gas from 500 to 1000 ppm.

From the XPS results of Ce 3d in Fig. 3(B), two multiplets (u and v) could be found after fitting. The bands labeled u1 and v1 represent

the 3d<sup>10</sup>4f<sup>1</sup> initial electronic state, corresponding to Ce<sup>3+</sup>, whereas the peaks labeled u, u2, u3, v, v2, and v3 represent the 3d<sup>10</sup>4f<sup>0</sup> state of Ce<sup>4+</sup> ions [24,25]. The Ce<sup>3+</sup> ratio, calculated by Ce<sup>3+</sup>/(Ce<sup>4+</sup> + Ce<sup>3+</sup>), was increased as a result of Ce–Fe/WMH exposure to SO<sub>2</sub>. Waqif et al. [26] reported that the SO<sub>2</sub> could act as a reducing agent, inducing a reduction from Ce<sup>4+</sup> to Ce<sup>3+</sup> on sample surface. All the spent Ce–Fe/WMH catalysts showed a little higher binding energies in Ce<sup>4+</sup> characteristic peaks than fresh catalyst (as shown in Table 1), indicating an expansion of CeO<sub>2</sub> fluorite lattice. Again, this was caused by the increase of Ce<sup>3+</sup>, whose effective ionic radius is about 14% larger than that of Ce<sup>4+</sup> in the same coordination [27]. According to the Yang et al. [28], the sulfation of CeO<sub>2</sub> could enhance the percent of Ce<sup>3+</sup> on catalyst surface, resulting in the formation of

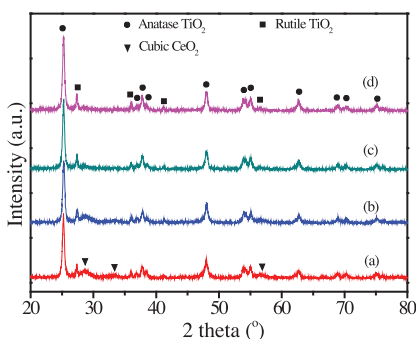


Fig. 2. XRD patterns of fresh and spent Ce–Fe/WMH catalysts. (a) fresh Ce–Fe/WMH, (b) Ce–Fe/WMH (100 ppm), (c) Ce–Fe/WMH (500 ppm), (d) Ce–Fe/WMH (1000 ppm).

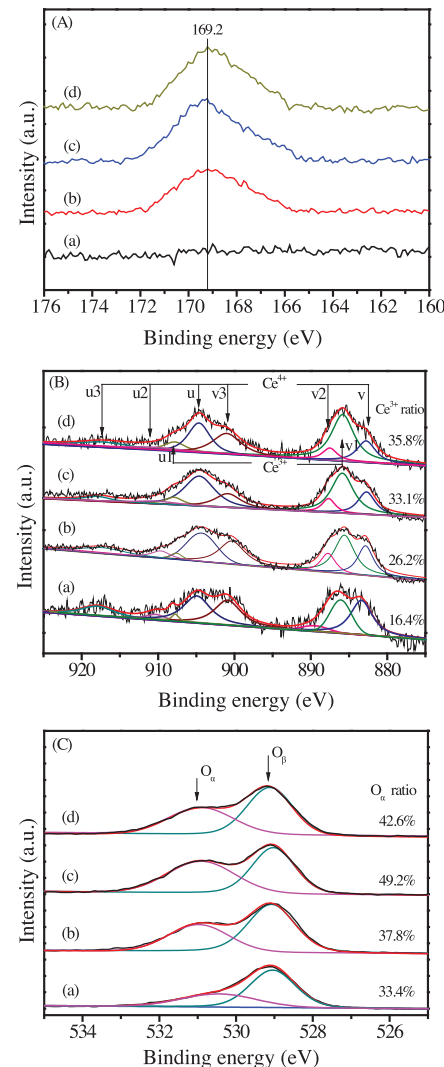


Fig. 3. XPS spectra of (A) S 2p, (B) Ce 3d and (C) O 1s of fresh and spent catalysts. (a) fresh Ce–Fe/WMH, (b) Ce–Fe/WMH (100 ppm), (c) Ce–Fe/WMH (500 ppm), (d) Ce–Fe/WMH (1000 ppm).

$\text{Ce}_2(\text{SO}_4)_3$ . Thus, it was thought that  $\text{Ce}_2(\text{SO}_4)_3$  was formed during the tested 100 h.

Fig. 3(C) revealed the fitted O 1s peaks for lattice oxygen  $\text{O}^{2-}$  at 529.0–529.3 eV (hereafter denoted as  $\text{O}_\beta$ ) and chemisorbed oxygen at 530.7–531.1 eV (hereafter denoted as  $\text{O}_\alpha$ ), such as  $\text{O}_2^{2-}$  and  $\text{O}^-$  belonging to defect-oxide or hydroxyl-like group [29]. All the spent Ce–Fe/WMH catalysts showed an increase of the ratio of  $\text{O}_\alpha/(\text{O}_\alpha + \text{O}_\beta)$  compared to fresh catalyst, suggesting the presence of more defect-oxide or hydroxyl-like group on the catalyst surface. It could be inferred that these surface hydroxyls were mainly acidic due to the hydration of  $\text{SO}_4^{2-}$  to form S–OH group, supplying more Brønsted acid sites to adsorb  $\text{NH}_3$  in the form of  $\text{NH}_4^+$  in the SCR reaction. This hypothesis would be verified by the following *in situ* DRIFTS experiments. In addition, the Fe 2p and Ti 2p XPS spectra were also recorded (as shown in Fig. S3). The binding energies of Fe 2p<sub>3/2</sub> (710.8 eV) and Fe 2p<sub>1/2</sub> (724.5 eV) corresponded well with the  $\text{Fe}^{3+}$  species, and the binding energies of Ti 2p<sub>3/2</sub> (458.6 eV) and Ti 2p<sub>1/2</sub> (464.5 eV) were typical characteristics of  $\text{Ti}^{4+}$  [30]. Comparing to the spectra of fresh Ce–Fe/WMH, the spectrum intensities of Fe 2p and Ti 2p became weak for the spent catalysts, suggesting a decrease of the Fe and Ti surface atomic concentration. Nonetheless, the binding energies of Fe 2p and Ti 2p remained unchanged before and after  $\text{SO}_2$  durability. It demonstrated that the iron or titanium species on catalyst surface was not sulfated during the tested 100 h, while the ceria was sulfated due to its higher binding energies in  $\text{Ce}^{4+}$  characteristic peaks after the reaction under  $\text{SO}_2$  environment. This could also be supported by the surface atomic concentrations of Ce, Fe and Ti (as shown in Table 1). After the tested 100 h, the decrease of surface Ce concentration was much lower than those of Fe and Ti, which suggested that the sulfation mainly occurred on ceria sites during the reaction.

The above-mentioned XPS results indicated that  $\text{SO}_2$  preferentially adsorbed on Ce sites during the tested 100 h, which could create more  $\text{Ce}^{3+}$  species on spent catalysts than those on fresh one. This would provide more oxygen vacancies on the catalyst surface and thus facilitate the activation and transportation of active oxygen species in reaction, which was beneficial to the SCR reaction.

TGA spectra of the fresh Ce–Fe/WMH, Ce–Fe/WMH (100 ppm), Ce–Fe/WMH (500 ppm), Ce–Fe/WMH (1000 ppm) and ammonium sulfate impregnated Ce–Fe/WMH catalysts are presented in Fig. 4. In the case of the fresh Ce–Fe/WMH, there was only one weight loss at 50–160 °C, which corresponded to  $\text{H}_2\text{O}$  desorption on the catalyst surface [31]. For spent catalysts, apart from the weight loss due to  $\text{H}_2\text{O}$  desorption, two new weight losses in the higher temperature range were also observed. The first small weight loss at 300–450 °C could be attributed to the decomposition of ammonium sulfate, and the second large weight loss at 670–800 °C was ascribed to the decomposition of metal sulfate (here  $\text{Ce}_2(\text{SO}_4)_3$ ) [11,31]. These results suggested that the reaction between oxidized  $\text{SO}_2$  and metal oxides predominated over the Ce–Fe/WMH in

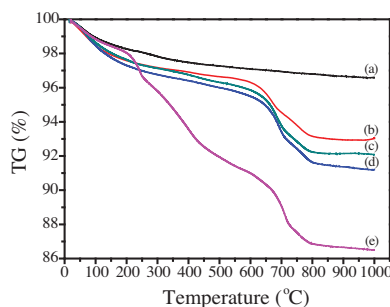


Fig. 4. TGA spectra of fresh and spent Ce–Fe/WMH catalysts. (a) Fresh Ce–Fe/WMH, (b) Ce–Fe/WMH (100 ppm), (c) Ce–Fe/WMH (500 ppm), (d) Ce–Fe/WMH (1000 ppm), (e) fresh Ce–Fe/WMH-containing ammonium sulfate.

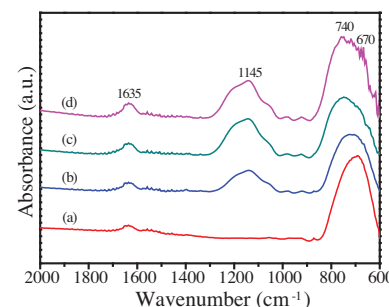


Fig. 5. FT-IR spectra of fresh and spent Ce–Fe/WMH catalysts. (a) fresh Ce–Fe/WMH, (b) Ce–Fe/WMH (100 ppm), (c) Ce–Fe/WMH (500 ppm), (d) Ce–Fe/WMH (1000 ppm).

the tested 100 h. In some literatures [11,31,32], the weight loss at relatively high temperatures due to the decomposition of metallic sulfates was thought to come from the decomposition of deposited ammonium sulfate during the heating course of the thermogravimetric analysis. Therefore, the impregnated ammonium sulfate on fresh Ce–Fe/WMH was also tested using TG to clarify how the sulfated  $\text{CeO}_2$  was formed on catalyst surface. The resulting TG curve exhibited three types of weight losses at similar temperature range to those of the spent catalysts. However, the intensity of weight loss due to the decomposition of ammonium sulfate was much higher than that of the spent catalysts, and the intensity of weight loss due to sulfated Ce was lower. This implied that the sulfated  $\text{CeO}_2$  was definitely formed by the reaction between oxidized  $\text{SO}_2$  and cerium oxides during the SCR reaction.

FT-IR spectra of the fresh and spent catalysts are showed in Fig. 5. All catalysts exhibited vibration absorptions at wave numbers of 1635, 740 and 670  $\text{cm}^{-1}$ , which could be attributed to different metal oxides [11]. Compared with the fresh Ce–Fe/WMH, the spent catalysts had a new adsorption at 1145  $\text{cm}^{-1}$ , indicating the existence of  $\text{SO}_4^{2-}$ . Free  $\text{SO}_4^{2-}$  ion shows usually two infrared-active peaks at 1140 and 626  $\text{cm}^{-1}$  [33], but the adsorption at 626  $\text{cm}^{-1}$  was overlapped by the absorptions of metal oxides. These results demonstrated that sulfate species should be formed during the SCR reaction in the presence of  $\text{SO}_2$ . Moreover, the IR adsorption intensity at 1145  $\text{cm}^{-1}$  exhibited little difference between Ce–Fe/WMH (500 ppm) and Ce–Fe/WMH (1000 ppm) but this adsorption was obviously larger than that for Ce–Fe/WMH (100 ppm). This suggested that the amount of  $\text{SO}_4^{2-}$  species slightly increased within the tested  $\text{SO}_2$  concentration (<1000 ppm). In addition, the band ascribed to the  $\text{NH}_4^+$  species was not detected, indicating the sulfur ammonium presented in a scarce amount beyond IR detection limits.

The specific surface areas of the fresh and spent catalysts are listed in Table 2. It showed clearly that the surface areas of all the spent Ce–Fe/WMH decreased after reactions in the presence of  $\text{SO}_2$ , which could be caused by formation/deposition of sulfated species on catalyst surface [13,34]. Yang et al. [28] reported that the surface area of  $\text{Ce}_2(\text{SO}_4)_3$  was lower than that of  $\text{CeO}_2$ . Combined with above results, the decrease of surface area of all the spent Ce–Fe/WMH was attributed to the formation of  $\text{Ce}_2(\text{SO}_4)_3$  during the tested 100 h. Furthermore, there was little difference

Table 2  
Specific surface areas of fresh and spent Ce–Fe/WMH catalysts.

Catalysts	BET surface area ( $\text{m}^2/\text{g}$ )
Fresh Ce–Fe/WMH catalyst	51.6
Ce–Fe/WMH catalyst (100 ppm)	41.1
Ce–Fe/WMH catalyst (500 ppm)	36.8
Ce–Fe/WMH catalyst (1000 ppm)	37.4

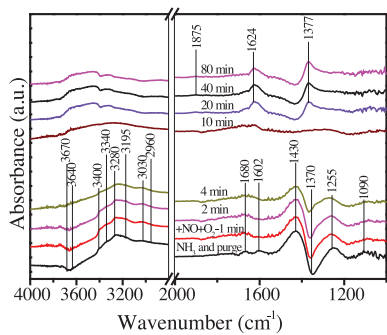


**Fig. 6.** In situ DRIFTS of reaction between  $\text{NO} + \text{O}_2$  and pre-adsorbed  $\text{NH}_3$  species at  $250^\circ\text{C}$  over Ce-Fe/WMH-S.

in surface area between Ce-Fe/WMH (500 ppm) and Ce-Fe/WMH (1000 ppm). It complied with the preceding demonstration that the formation of sulfated  $\text{CeO}_2$  on catalyst surface might approach a stable state upon certain amount of  $\text{SO}_2$  in reactant gas. It was noteworthy that the  $\text{NO}_x$  conversion variation trends in the first 50 min and following reaction time were different, both of which might be controlled by different mechanisms. The detailed SCR reaction mechanism over Ce-Fe/WMH-sulfation would be further investigated using in situ DRIFTS method in the following section.

### 3.3. Reaction mechanism over Ce-Fe/WMH-sulfation

In mechanism study, the fresh Ce-Fe/WMH was first pre-treated in a flow of 1000 ppm  $\text{SO}_2 + 3\% \text{O}_2$  for 100 h, and then applied to DRIFTS analysis. The resulting sample was denoted as Ce-Fe/WMH-S. Fig. 6 shows the in situ DRIFTS spectra of the reaction between  $\text{NO} + \text{O}_2$  and pre-adsorbed  $\text{NH}_3$  species on Ce-Fe/WMH-S at  $250^\circ\text{C}$ . After  $\text{NH}_3$  adsorption and  $\text{N}_2$  purge at  $250^\circ\text{C}$ , the catalyst surface was mainly covered by ionic  $\text{NH}_4^+$  ( $\delta_s$  at  $1680\text{ cm}^{-1}$  and  $\delta_{as}$  at  $1430\text{ cm}^{-1}$ ) bound to Brønsted acid sites and coordinated  $\text{NH}_3$  ( $\delta_s$  at  $1255\text{ cm}^{-1}$  and  $\delta_{as}$  at  $1602\text{ cm}^{-1}$ ) bound to Lewis acid sites [35,36]. At the same time, N-H stretching vibration modes from ionic  $\text{NH}_4^+$  ( $3280, 3030$  and  $2960\text{ cm}^{-1}$ ) [37] and coordinated  $\text{NH}_3$  ( $3400, 3340$  and  $3195\text{ cm}^{-1}$ ) [38] also appeared, together with the negative bands at  $3670$  and  $3640\text{ cm}^{-1}$  due to the hydroxyl consumption through interaction with  $\text{NH}_3$  to form  $\text{NH}_4^+$ . The intense negative band at  $1370\text{ cm}^{-1}$  ( $\nu_{asS-O}$ ) was caused by the interaction between sulfate species and  $\text{NH}_3$ , in which ammonium sulfate might form on the catalyst surface. The band at  $1090\text{ cm}^{-1}$  might be attributed to the perturbation of sulfate species ( $\nu_{SS-O}$ ) through reaction with  $\text{NH}_3$  to form ammonium sulfate [39]. After the introduction of  $\text{NO} + \text{O}_2$ , the bands ascribed to ionic  $\text{NH}_4^+$  and coordinated  $\text{NH}_3$  showed an obvious decrease in intensity and totally disappeared after 10 min, implying that the adsorbed  $\text{NH}_3$  species could react with  $\text{NO} + \text{O}_2$ . Meanwhile, the negative band at  $1370\text{ cm}^{-1}$  was recovered, suggesting that the  $\text{NH}_4^+$  bound to sulfate species could also take part in the SCR reaction. This could explain the reason for the low ammonium sulfate deposition on catalyst surface during the SCR reaction in the presence of  $\text{SO}_2$ . With the reaction time continuous increase, two new bands at  $1377$  and  $1624\text{ cm}^{-1}$  appeared. They were assigned to the deposited sulfate species ( $\nu_{asS-O}$ ) and adsorbed  $\text{H}_2\text{O}$  produced in the SCR reaction [40], respectively. These results suggested that  $\text{NO} + \text{O}_2$  readily reacted with the adsorbed  $\text{NH}_3$  species on Ce-Fe/WMH-S. After the pre-adsorbed  $\text{NH}_3$  species were consumed, a new band at  $1875\text{ cm}^{-1}$  attributed to gaseous  $\text{NO}$  [41] showed up.

Afterwards, the in situ DRIFTS measurement of reaction between  $\text{NH}_3$  and pre-adsorbed  $\text{NO}_x$  species over Ce-Fe/WMH-S was carried out and the results are shown in Fig. 7. After  $\text{NO} + \text{O}_2$  adsorption and  $\text{N}_2$  purge at  $250^\circ\text{C}$ , two slight bands assigned to  $\text{NO}_2$

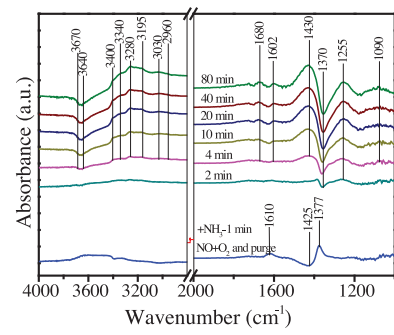


**Fig. 7.** In situ DRIFTS of reaction between  $\text{NH}_3$  and pre-adsorbed  $\text{NO}_x$  species at  $250^\circ\text{C}$  over Ce-Fe/WMH-S.

( $1610\text{ cm}^{-1}$ ) and deposited sulfate species ( $\nu_{asS-O}$ ) ( $1377\text{ cm}^{-1}$ ) appeared [41,42]. The negative band at  $1425\text{ cm}^{-1}$  could be assigned to the displacement of the sulfate species, implying that  $\text{NO}$  and  $\text{SO}_2$  were adsorbed competitively on catalyst surface. The subsequent introduction of  $\text{NH}_3$  resulted in the accumulation of adsorbed  $\text{NH}_3$  species on catalyst surface, including ionic  $\text{NH}_4^+$  ( $\delta_s$  at  $1680\text{ cm}^{-1}$  and  $\delta_{as}$  at  $1430\text{ cm}^{-1}$ ) and coordinated  $\text{NH}_3$  ( $\delta_s$  at  $1255\text{ cm}^{-1}$  and  $\delta_{as}$  at  $1602\text{ cm}^{-1}$ ), similar to the results shown in Fig. 6. During the whole process, the band at  $1624\text{ cm}^{-1}$  corresponding to adsorbed  $\text{H}_2\text{O}$  could hardly be detected. It indicated that the reaction between  $\text{NH}_3$  and adsorbed  $\text{NO}_x$  species on Ce-Fe/WMH-S might be neglected.

Finally, the in situ DRIFTS measurement of SCR reaction over Ce-Fe/WMH-S as a function of time was conducted and the results are shown in Fig. 8. During the whole reaction process, only adsorbed  $\text{NH}_3$  species were detected on catalyst surface, except for a weak band at  $1875\text{ cm}^{-1}$  due to gaseous  $\text{NO}$ . This result showed that the reaction between adsorbed  $\text{NH}_3$  and gaseous  $\text{NO}$  occurred on the Ce-Fe/WMH-S.

According to the above in situ DRIFTS results, it could be observed that most active sites were covered by adsorbed  $\text{NH}_3$  species during the whole reaction process, and Brønsted acid sites and Lewis acid sites served as important active sites. In this way,  $\text{NH}_3$ -SCR reaction of Ce-Fe/WMH-S might take place via an Eley-Rideal (E-R) type mechanism, where ionic  $\text{NH}_4^+$  and coordinated  $\text{NH}_3$  reacted with gaseous  $\text{NO}$ . During this process, the dehydrogenation of ionic  $\text{NH}_4^+$  and coordinated  $\text{NH}_3$  to  $\text{NH}_2$  intermediate species by active oxygen species might be the rate determining step, followed by subsequent reaction with  $\text{NO}$  to produce  $\text{H}_2\text{O}$  and  $\text{N}_2$ . In addition, the DRIFTS spectra of  $\text{NH}_3$  adsorption on Ce-Fe/WMH-S and fresh Ce-Fe/WMH at  $250^\circ\text{C}$  were also recorded (as shown in Fig. S4(A)). It revealed that the amount of ionic  $\text{NH}_4^+$  increased greatly after sulfation, which was in accordance with the above assumption that the Brønsted acidity was enhanced after sulfation (as shown in XPS results), but

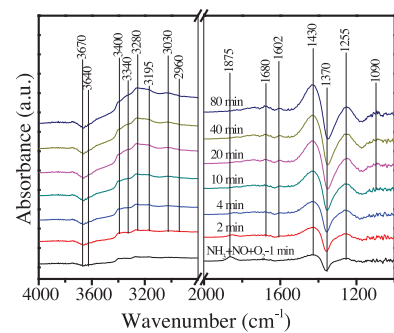


**Fig. 8.** In situ DRIFTS of reaction in  $\text{NO} + \text{O}_2 + \text{NH}_3$  at  $250^\circ\text{C}$  over Ce-Fe/WMH-S.

the coordinated NH<sub>3</sub> was little influenced by SO<sub>2</sub>. The enhanced Brønsted acidity was mainly resulted from SO<sub>4</sub><sup>2-</sup> on catalyst surface. Above all, the enhancement of Brønsted acidity and the increase of active oxygen species on catalyst surface caused by sulfation might be the important reason for the good SCR performance in SO<sub>2</sub>-containing gas over Ce-Fe/WMH.

Some researchers [43,44] reported that both the E-R mechanism (i.e. reaction of activated NH<sub>3</sub> species with gaseous NO) and the Langmuir-Hinshelwood (L-H) mechanism (i.e. reaction of adsorbed NO<sub>x</sub> species with adsorbed NH<sub>3</sub> species) might happen during the SCR reaction over catalysts. In this work, the NO<sub>x</sub> adsorption capability of Ce-Fe/WMH-S was much weaker than that of fresh Ce-Fe/WMH (as shown in Fig. S4(B)), and the reaction between adsorbed NO<sub>x</sub> and NH<sub>3</sub> species on Ce-Fe/WMH-S was neglected (as shown in Fig. 7). Thus, it suggested that the L-H reaction pathway was cut off due to the sulfation process, which might result in the rapid decrease of NO<sub>x</sub> conversion in the early period of SCR reaction in the presence of SO<sub>2</sub> (as shown in Fig. 1).

#### 4. Conclusions

The SO<sub>2</sub> durability of the Ce-Fe/WMH was greatly improved by surface sulfation. From various characterizations, it was observed that sulfation could result in an enrichment of Ce<sup>3+</sup> on catalyst surface and induced much Brønsted acid sites, both of which were conductive to SCR activity. Accordingly, the mechanism study showed that only the E-R reaction pathway dominated in the NH<sub>3</sub>-SCR reaction over sulfated Ce-Fe/WMH, which was an important reason for its enhanced SO<sub>2</sub> durability at 250 °C. For practical use, this Ce-Fe/WMH catalyst can be used for deNO<sub>x</sub> process in the presence of SO<sub>2</sub>.

#### Acknowledgments

This work was supported by the National Basic Research Program of China (973 Program) (No. 2011CB936002) and National Innovation Experiment Program for University Students.

#### Appendix A. Supplementary data

Supplementary material related to this article can be found, in the online version, at <http://dx.doi.org/10.1016/j.apcatb.2014.01.008>.

#### References

- [1] L.J. Alemany, F. Berti, G. Busca, G. Ramis, D. Robba, G.P. Toledo, M. Trombetta, *Applied Catalysis B: Environmental* 10 (1996) 299–311.
- [2] G. Busca, L. Lietti, G. Ramis, F. Berti, *Applied Catalysis B: Environmental* 18 (1998) 1–36.
- [3] M. Kobayashi, K. Miyoshi, *Applied Catalysis B: Environmental* 72 (2007) 253–261.
- [4] M.S. Kumar, W. Grünert, A. Brückner, *Journal of Catalysis* 239 (2006) 173–186.
- [5] H. Sjövall, L. Olsson, E. Fridell, R.J. Blint, *Applied Catalysis B: Environmental* 64 (2006) 180–188.
- [6] W.Q. Xu, Y.B. Yu, C.B. Zhang, H. He, *Catalysis Communications* 9 (2008) 1453–1457.
- [7] G. Qi, R.T. Yang, *Applied Catalysis B: Environmental* 44 (2003) 217–225.
- [8] P. Li, Y. Xin, Q. Li, Z.P. Wang, L.R. Zheng, *Environmental Science and Technology* 46 (2012) 9600–9605.
- [9] Y. Shu, H. Sun, X. Quan, S. Chen, *Journal of Physical Chemistry C* 116 (2012) 25319–25327.
- [10] W.S. Kijlstra, M. Biervliet, E.K. Poels, A. Bliek, *Applied Catalysis B: Environmental* 16 (1998) 327–337.
- [11] J. Yu, F. Guo, Y.L. Wang, Y.L. Liu, S.Q. Gao, *Applied Catalysis B: Environmental* 95 (2010) 160–168.
- [12] Y. Cheng, C. Lambert, D.H. Kim, J.H. Kwak, S.J. Cho, C.H.F. Peden, *Catalysis Today* 151 (2010) 266–270, 151.
- [13] Z.P. Zhu, Z.Y. Liu, H.X. Niu, S.J. Liu, *Journal of Catalysis* 187 (1999) 245–248.
- [14] R.Q. Long, R.T. Yang, *Journal of Catalysis* 186 (1999) 254–268.
- [15] Y.Q. Hou, Z.G. Huang, S.J. Guo, *Catalysis Communications* 10 (2009) 1538–1541.
- [16] R.B. Jin, Y. Liu, Z.B. Wu, T.T. Gu, *Catalysis Today* 153 (2010) 84–89.
- [17] J. Chen, R.T. Yang, *Journal of Catalysis* 139 (1993) 277–288.
- [18] R.Q. Long, M. Chang, R.T. Yang, *Applied Catalysis B: Environmental* 33 (2001) 97–107.
- [19] E. García-Bordejé, J.L. Pinilla, M.J. Lázaro, R. Moliner, *Journal of Catalysis* 233 (2005) 166–175.
- [20] H. Sun, X. Quan, S. Chen, H.M. Zhao, *Applied Surface Science* 253 (2007) 3303–3310.
- [21] Y. Shu, H. Sun, X. Quan, S. Chen, *Industrial Engineering Chemical Research* 51 (2012) 7867–7873.
- [22] M.Y. Smirnov, A.V. Kalinkin, A.V. Pashis, K.C. Kharas, V.I. Bukhtiyarov, *Journal of Physical Chemistry B* 109 (2005) 11712–11719.
- [23] G. Xie, Z.Y. Liu, Z.P. Zhu, Q. Liu, *Journal of Catalysis* 224 (2004) 42–49.
- [24] F.B. Noronha, E.C. Fendley, R.R. Soares, W.E. Alvarez, D.E. Resasco, *Chemical Engineering Journal* 82 (2001) 21–31.
- [25] H. He, H. Dai, C.T. Au, *Catalysis Today* 90 (2004) 245–254.
- [26] M. Waqif, P. Bazin, O. Saur, J.C. Lavalley, O. Touret, *Applied Catalysis B: Environmental* 11 (1997) 193–205.
- [27] P. Dutta, S. Pal, M.S. Seehra, *Chemistry of Materials* 18 (2006) 5144–5146.
- [28] S.J. Yang, Y.F. Guo, H.Z. Chang, L. Ma, Y. Peng, Z. Qu, N.Q. Yan, C.Z. Wang, J.H. Li, *Applied Catalysis B: Environmental* 136–137 (2013) 19–28.
- [29] J.C. Dupin, D. Gonbeau, P. Vinatier, A. Levasseur, *Physical Chemistry Chemical Physics* 2 (2000) 1319–1324.
- [30] S. Roy, B. Viswanath, M.S. Hegde, G. Madras, *Journal of Physical Chemistry C* 112 (2008) 6002–6012.
- [31] J.H. Huang, Z.Q. Tong, Y. Huang, J.F. Zhang, *Applied Catalysis B: Environmental* 78 (2008) 309–314.
- [32] Z.B. Wu, R.B. Jin, H.Q. Wang, Y. Liu, *Catalysis Communications* 10 (2009) 935–939.
- [33] K. Nakamoto, *Infrared Raman Spectra of Inorganic and Coordination Compounds*, fourth ed., Wiley, New York, NY, 1986.
- [34] Z.G. Huang, Z.P. Zhu, Z.Y. Liu, *Applied Catalysis B: Environmental* 39 (2002) 361–368.
- [35] R.Q. Long, R.T. Yang, *Journal of Catalysis* 207 (2002) 224–231.
- [36] B. Guan, H. Lin, L. Zhu, *Journal of Physical Chemistry C* 115 (2011) 12850–12863.
- [37] S. Gopalakrishnan, P. Jungwirth, D.J. Tobias, H.C. Allen, *Journal of Physical Chemistry B* 109 (2005) 8861–8872.
- [38] G. Piazzesi, O. Kröcher, M. Elsener, A. Wokaun, *Applied Catalysis B: Environmental* 65 (2006) 55–61.
- [39] F.D. Liu, K. Asakura, H. He, W.P. Shan, X.Y. Shi, C.B. Zhang, *Applied Catalysis B: Environmental* 103 (2011) 369–377.
- [40] G.S. Qi, R.T. Yang, *Journal of Physical Chemistry B* 108 (2004) 15738–15747.
- [41] G. Ramis, L. Yi, G. Busca, M. Turco, E. Kotur, R.J. Willey, *Journal of Catalysis* 157 (1995) 523–535.
- [42] B.Q. Jiang, Z.B. Wu, Y. Liu, S.C. Lee, W.K. Ho, *Journal of Physical Chemistry C* 114 (2010) 4961–4965.
- [43] S.J. Yang, J.H. Li, S.Z. Wang, J.H. Chen, L. Ma, *Applied Catalysis B: Environmental* 117 (2012) 73–80.
- [44] S. Yang, C. Wang, J.H. Li, N.Q. Yan, L. Ma, H.Z. Chang, *Applied Catalysis B: Environmental* 110 (2011) 71–80.